Remote Sensing of Environment 128 (2013) 224–233

Contents lists available at SciVerse ScienceDirect

Remote Sensing of Environment

journal homepage: www.elsevier.com/locate/rse

Estimation of the diffuse attenuation coefficient K_{dPAR} using MERIS and application to seabed habitat mapping

Bertrand Saulquin [a,*], Anouar Hamdi [b], Francis Gohin [c], Jacques Populus [c], Antoine Mangin [a], Odile Fanton d'Andon [a]

[a] ACRI-ST, Sophia-Antipolis, France
[b] Institut des Milieux Aquatiques, Bayonne, France
[c] Ifremer, Brest, France

ARTICLE INFO

Article history:
Received 25 August 2011
Received in revised form 27 September 2012
Accepted 6 October 2012
Available online 9 November 2012

Keywords:
Ocean color
Light attenuation
Photosynthetic available radiation
Euphotic depth
Seabed mapping

ABSTRACT

The availability of light in the water column and at the seabed determines the euphotic zone and constrains the type and the vertical distribution of algae species. Light attenuation is traditionally quantified as the diffuse attenuation coefficient of the downwelling spectral irradiance at wavelength 490 nm (K_{d490}) or the photosynthetically available radiation (K_{dPAR}). Satellite observations provide global coverage of these parameters at high spatial and temporal resolution and several empirical and semi-analytical models are commonly used to derive K_{d490} and K_{dPAR} maps from ocean colour satellite sensors. Most of these existing empirical or semi-analytical models have been calibrated in open ocean waters and perform well in these regions, but tend to underestimate the attenuation of light in coastal waters, where the backscattering caused by the suspended matters and the absorption by the dissolved organic matters increase light attenuation in the water column.

We investigate two relationships between K_{dPAR} and K_{d490} for clear and turbid waters using MERIS reflectances and the spectral diffuse attenuation coefficient $K_d(\lambda)$ developed by Lee (2005). Satellite-derived fields of K_{d490} and modelled K_{dPAR} are evaluated using coincident in-situ data collected over the world in both clear and turbid waters, and by using Ecolight simulations. Temporal means at 250 m resolution of K_{dPAR} and euphotic depth were computed over the period 2005–2009 for European coastal waters. These mean data were cross-tabulated with in-situ data of kelp (*Laminaria hyperborea*) and seagrass (*Posidonia oceanica*), respectively observed at locations on Atlantic and Mediterranean shores where the light is taken as the limiting factor to the depth distribution for these species. The minima observed for *P. oceanica*, in percent of energy, are very close to 1% of surface irradiance, the historical threshold known as euphotic depth as defined by Ryther (1956). Real estimates of the surface irradiance (Frouin, 1989) are used in conjunction with the estimated K_{dPAR} to calculate the residual energy at the lower limit of *P. oceanica* and *L. hyperborea* in mol·photons·m^{-2}·day^{-1} as a complement to the usual fraction of the surface energy. We show that the observed values, in terms of energy, for both species were equivalent to the values reported in the literature.

1. Introduction

The light available in the water column at wavelengths between 400 and 700 nm in the visible part of the spectrum, termed photosynthetically active radiation (PAR), is utilised by phytoplankton for photosynthesis (Falkowski & Raven, 1997; Kirk, 1994) and constrains the type and distribution of algae species and benthic algae, which contribute significantly to total primary production (Cahoon et al., 1993; McMinn et al., 2005; Carter et al., 2005). The estimation of the light attenuation in the water column is also critical to understand physical processes such as the heat transfer in the upper layer of the ocean (Lewis et al., 1990; Morel & Smith, 1974; Sathyendranath et al., 1991; Rocheford et al., 2001; Wu et al., 2007). From an optical perspective, in addition to pure water, light attenuation is constrained by the concentration of three components (IOCCG Report 3, 2000): pigments, expressed here as the concentration of chlorophyll-a ([Chl-a]), dissolved yellow substances (gelbstoff or CDOM) absorption a_{cdm} and suspended particulate matter concentration ([SPM]). The in-situ spectral diffuse attenuation coefficient $K_d(\lambda)$ was traditionally measured by the ocean-colour scientific community at 490 nm (K_{d490}), following the primary studies in the 1970s (Jerlov, 1976). Concurrently, biologists have focused on the PAR measurement and attenuation (K_{dPAR}). Both K_{dPAR} and K_{d490} increase with increasing solar zenith angle and K_{dPAR} is significantly depth dependent (the longer wavelength, red in this example, is rapidly attenuated in the water column relatively to the shorter wavelength blue) even for well-mixed waters.

Since the launch of the Coastal Zone Color Scanner (CZCS) in 1978, the ocean-colour community has provided maps of K_{d490} or K_{dPAR} at large spatial scales offering a great improvement in spatial and temporal

* Corresponding author. Tel.: +33 492967128.
E-mail address: bertrand.saulquin@acri-st.fr (B. Saulquin).

0034-4257/$ – see front matter © 2012 Elsevier Inc. All rights reserved.
http://dx.doi.org/10.1016/j.rse.2012.10.002

resolution compared to in-situ data. Space based sensors measure top-of-atmosphere radiances at different wavelengths and the Medium Resolution Imaging Spectrometer (MERIS) sensor has 15 bands between 412 and 865 nm. The contribution from the atmosphere is firstly removed from the top-of-atmosphere radiance, through a process known as atmospheric correction (Gordon & Wang, 1994), to obtain the water-leaving radiance (Lw). The Lw values are normalised, i.e. expressed in standard solar conditions (sun at zenith) in the absence of the atmosphere, and corrected for bidirectional effects (viewing angle dependence and effects of seawater anisotropy, Morel et al., 2002) to obtain the normalised water-leaving radiance (nLw). Today, several empirical and semi-analytical models of K_{d490} and K_{dPAR} are commonly used to derive K_{d490} maps from satellite-derived nLw.

Mueller (2000) defines an empirical relationship between K_{d490} and the ratio between blue and green water-leaving radiances from the Sea-viewing Wide Field-of-view Sensor (SeaWiFS) (McClain et al., 2004), and the Moderate Resolution Imaging Spectroradiometer (MODIS) (Esaias et al., 1998). Morel et al. (2007) proposes an empirical relationship between the K_{d490} and the Chl-a concentration. Lee et al. (2002, 2005a, 2005b, 2007) provided a semi-analytical model for K_{d490} with dedicated versions for SeaWiFS, MERIS and MODIS nLw.

K_{dPAR} has historically been expressed as a function of [Chl-a] (Morel, 1988) for clear open ocean waters. This latest approach is routinely used in the open ocean where phytoplankton is the main contributor to attenuation (Claustre & Maritorena, 2003). In coastal waters however, the determination of K_{dPAR} is complicated by increased light attenuation by CDOM and SPM(Case 2 waters). In coastal areas regional approaches express K_{dPAR} as a function of the [Chl-a], and [SPM] (Devlin et al., 2009; Gohin et al., 2005). More recently, K_{dPAR} is more often related to K_{d490} using empirical approaches and the relationship between K_{d490} and K_{dPAR} has quite large regional variations (Barnard et al., 1999; Pierson, 2008; Morel et al., 2007; Pierson et al., 2008; Wang et al., 2009; Zaneveld et al., 1993).

In this paper, we show the performance of three models of K_{d490} (Lee et al., 2005a, 2005b; Morel et al., 2007; Mueller, 2000), routinely used as standard MERIS, SeaWiFS and MODIS Level 3 products, compared to an in-situ dataset collected near shore and in clear open ocean waters. We then derive two relationships between K_{dPAR} and K_{d490}, estimated by integrating the spectral irradiances over the euphotic depth and the visible spectrum using $K_d(\lambda)$ as estimated using Lee et al. (2005a, 2005b).

Our aim is to provide an estimation of K_{dPAR} for values greater than 0.06 m^{-1} and lower than 1 m^{-1}. For more turbid waters, dedicated algorithms may be used, and for oligotrophic waters ($K_{dPAR}<0.06$ m^{-1}), standard K_{dPAR} estimations (Morel et al., 2007; Mueller, 2000) are freely available at 4 km resolution on the Globcolour website (www.globcolour.info), and the oceancolor webpage (http://oceancolor.gsfc.nasa.gov/).

Secondly, temporal means of satellite derived K_{dPAR} and Z_{eu} were calculated for the European waters, from 2005 to 2009, to characterise a reference state for light and marine coastal fauna and flora in the intertidal zone at 250 m resolution.

Finally, six sites where selected by Ifremer in Corsica (Mediterranean Sea) and in Brittany (English Channel and Atlantic Ocean) to compare the satellite derived minimum light threshold values for *P. oceanica* and *L. hyperborea* to the literature. The threshold of 1% used to define Z_{eu} as the minimum light requirement for benthic primary production, was historically determined from in-situ observations of *P. oceanica* in the Mediterranean Sea. We therefore compare the satellite-derived 1% to the deepest depth at which *P. oceanica* is observed at the Corsican site. Nevertheless, some species can survive at lower light levels and the evaluation of the light available in fraction of the surface irradiance is biologically meaningless (Gattuso et al., 2006) as the fraction of moonlight is the same than the fraction of sunlight. Therefore, we propose the use of daily integrated PAR (Frouin et al., 1989) attenuated into the water column using K_{dPAR}, to arrive at an estimation of the PAR in the water column in $\mathrm{mol \cdot photons \cdot m^{-2} \cdot d^{-1}}$. This provides a more meaningful estimation of energy in the water column than fraction of the surface energy, generally used by the community.

2. Methods

The spectral diffuse attenuation coefficient $K_d(\lambda)$ is the coefficient of the exponential attenuation of the spectral downwelling irradiance:

$$Ed(\lambda) = E0(\lambda).e^{-Kd(\lambda)z}. \tag{1}$$

Here $E_d(\lambda)$ is the spectral downwelling irradiance in $W.m^{-2}.nm^{-1}$ at depth z and wavelength λ and $E_0(\lambda)$ is the energy just beneath the surface). All symbols and acronyms cited in the text are summarized in Table 1 for a better understanding. If the visible spectral domain is considered, the PAR at depth z can be related to $K_d(\lambda)$ and E_d (λ) using energetic (Eq. 2a) or quantum units (Eq. 2b.) (Baker & Frouin, 1987; Morel & Smith, 1974):

$$\mathrm{PAR}(z) = \int_{400\mathrm{nm}}^{700\mathrm{nm}} \mathrm{Ed}(\lambda; z=0).\exp^{-\mathrm{Kd}(\lambda).z} d\lambda \left[\mathrm{W.m^{-2}}\right] \tag{2a}$$

$$\mathrm{PAR}(z) = \frac{1}{h.c}\int_{400\mathrm{nm}}^{700\mathrm{nm}} \lambda.\mathrm{Ed}(\lambda; z=0).\exp^{-\mathrm{Kd}(\lambda).z} d\lambda \left[\mathrm{photons.m^{-2}.s^{-1}}\right]. \tag{2b}$$

An expression of the instantaneous $K_{dPAR}(z)$ is:

$$\mathrm{KdPAR}(z) = -\frac{\ln(\mathrm{PAR}(z+dz)) - \ln(\mathrm{PAR}(z))}{dz}. \tag{3}$$

K_{dPAR} changes with depth as the red photons are absorbed in the top layers. The spectral diffuse attenuation coefficient of downwelling irradiance $K_d(\lambda)$ also changes with depth, but its magnitude of variation is significantly smaller than that of K_{dPAR} (Lee, 2009; Zaneveld et al., 1993). The Hydrolight/Ecolight (© Curtis D. Mobley, 2008) is a radiative transfer model that computes radiance distributions and related quantities (irradiance, reflectances, diffuse attenuation functions, etc.) in any water body starting from the Chl-a and SPM concentration and CDOM absorption. Fig. 1 shows two Ecolight simulations of K_{dPAR} for clear (blue plot) and coastal turbid waters (orange plot). In this simulation the water is assumed to be well mixed and scattering of particulates is based on the model of Gordon and Morel (1983). The sky is assumed to be cloudless

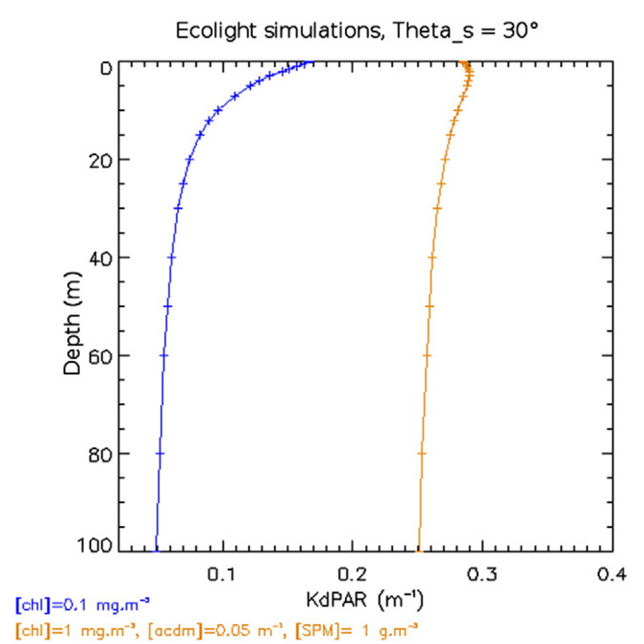

Fig. 1. Simulated $K_{dPAR}(z)$ in the water column using Ecolight for clear water with low [Chl-a] (case1, blue) and coastal water (case 2, orange).

with the sun at 30° from the zenith. For coastal water simulation (orange), [Chl-a] is set to 1 $mg \cdot m^{-3}$, a_{cdom} to 0.05 m^{-1} and [SPM] to 1 $g \cdot m^{-3}$. The instantaneous K_{dPAR} (Fig. 1) is estimated using Eq. (3). Fig. 1 verifies that $K_{dPAR}(z)$ is more constant for coastal turbid waters (Wang et al., 2009).

We consider in this paper the vertical average value of K_{dPAR} between the surface and the euphotic depth, $\overline{KdPAR}$ (Eq. 4) because K_{dPAR} values reported in the literature or in-situ databases used for validation are estimated using Eq. (5) in this expression.

$$\overline{KdPAR} = \frac{\ln(PAR(0)) - \ln(PAR(z))}{z} \tag{4}$$

We use $z = Z_{eu}$ in this study. Using $\overline{KdPAR}$, instead of $K_{dPAR}(z)$ will lead to an accurate estimation of PAR near the surface and Z_{eu}. Between these two depths, PAR will be slightly over-estimated. Further in this paper, $\overline{KdPAR}$ is noted K_{dPAR}.

3. In-Situ data

3.1. K_{d490}, K_{dPAR} measurements

In-situ Ed(λ,z) or PAR(z) measurements must be collected following a community-vetted protocol, (Werdell & Bailey, 2005a, 2005b) to avoid ship shadow and reflectance. If required (not here), PAR irradiance data expressed in $W \cdot m^{-2}$ can be converted to molar units using the following approximation: 2.5×10^{18} $quanta \cdot s^{-1} \cdot W^{-1}$ or 4.2 $\mu E \cdot m^{-2} \cdot s^{-1} \cdot W^{-1}$ (Morel & Smith, 1974). In-situ data of K_{d490} and K_{dPAR} available through global datasets such as NOMAD (http://seabass.gsfc.nasa.gov/data/nomad_seabass_v2.a_2008200.txt), SeaBASS (http://seabass.gsfc.nasa.gov/) were extracted over the period 2005 to 2009.

Data from the instrumented buoy BOUSSOLE located near Villefranche (France) in the Mediterranean sea were also used (http://www.upmc.fr/en/research/living_earth_and_environment_section/laboratories/villefranche_sur_mer_oceanography_laboratory_umr_7093.html). Additional data in the Cheasapeake Bay, which is traditionally a turbid area (Wang & Shi, 2005), and data obtained from Ifremer and OPTIC-MED (2008) and OPTIC-PCAF (2004) cruises were also added as they provide some in-situ measurements on shores where SPM backscattering and CDOM absorption may be important.

In-situ K_{d490} and K_{dPAR} values reported in public databases are calculated using Eq. (4) and integrated over the first optical depth of E_{d490} (Z_{90}–$1/K_{d490}$) (Morel et al., 2007). To validate either satellite-derived K_{d490} or K_{dPAR}, we produced "matchups", i.e., data pairs of satellite-derived K_d and in-situ collocated in space (same pixel) and obtained during the same day. The satellite K_{d490} (Figs. 2 to 6) is directly comparable to the in-situ $K_{d490.}$ We estimated, using Ecolight and the IOP available for the matchups from NOMAD and Seabass dataset, a correction for $K_{dPAR}(Z_{eu}) = 0.94 * K_{dPAR}(Z_{90})$ as we do not have the irradiance profiles to re-estimate $K_{dPAR}(Z_{eu})$. This correction is applied to Figs. 7a and 9. For OPTICs (12 matchups of Fig. 7) and Ifremer dataset (18 matchups of Fig. 7), the higher values of Fig. 7, we calculated $K_{dPAR}(Z_{eu})$ from the irradiance profiles and Eq. (4).

Matchups are used to produce statistical comparisons for the two fields. Bias and Pearson correlation coefficient (R) for Figs. 2 to 7 are calculated on log-transformed data.

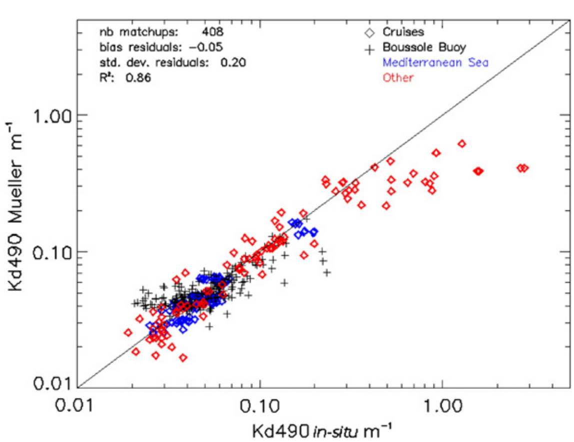

Fig. 2. Mueller's K_{d490} vs. in-situ.

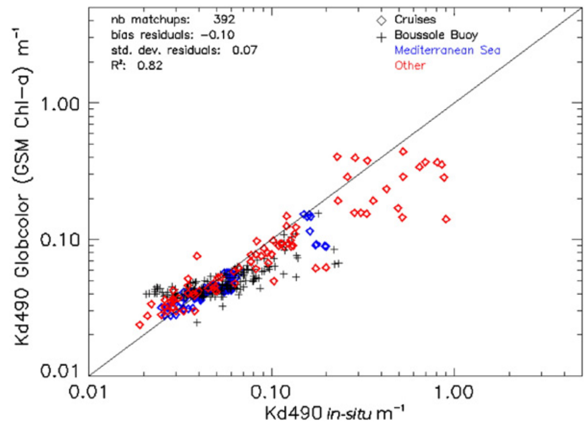

Fig. 3. Morel's K_{d490} vs. in-situ.

3.2. Seagrass and kelp data

In-situ coverage of *P. oceanica* in Corsica and single beam sounder survey data acquired on rocky seabed covered by kelp (*L. hyperborea*) in Brittany (Méléder et al., 2010), are used to compare satellite-derived residual energy observed at the macrophytes lower limits to the known minimum thresholds reported in the literature. Six sites were selected by Ifremer according to accurate knowledge of species distribution and state of conservation, and the availability of an accurate bathymetry (resolution of 100 m horizontally and 1 to 5 m vertically).

Table 1
List of symbols and abbreviations.

Symbol	Definition	Unit
Lw	Water leaving radiance	$W \cdot m^{-2} \cdot sr^{-1} \cdot m^{-1}$
a(λ)	Absorption coefficient at wavelength λ	m^{-1}
bb (λ)	Backscattering coefficient at wavelength λ	m^{-1}
CDOM	Coloured dissolved organic matters	
Chl-a	Chlorophyll-a	
DTM	Digital terrain model	
GSM	Garver–Siegel–Maritorena	
Globcolour	Global ocean colour ESA funded project	
SPM	Suspended particulate matter	
$E_d(\lambda, z)$	Spectral downwelling irradiance at depth z	$W \cdot m^{-2} \cdot m^{-1}$
IOP	Inherent optical properties	
$K_d(\lambda, E\%)$	Spectral diffuse attenuation coefficient for downwelling irradiance between $E_d(\lambda,0)$ and % of E_d (λ,0)	m^{-1}
K_{dPAR}	Diffuse attenuation coefficient of PAR	m^{-1}
$\overline{KdPAR}$	Vertical average value of mean diffuse attenuation coefficient over the euphotic layer	m^{-1}
MERIS	Medium resolution imaging spectrometer	
MODIS	Moderate resolution imaging spectroradiometer	
PAR	Photosynthetically available radiation	$photons \cdot m^{-2} \cdot s^{-1}$ or $W \cdot m^{-2}$
Rrs	Remote sensing reflectance (ratio of water-leaving radiance to downwelling irradiance above the surface)	
SHOM	Service Hydrographique et Océanographique de la Marine	
SeaWiFS	Sea-viewing wide field-of-view sensor	
Z_{eu}	Euphotic depth	m
Z_{490}	Depth at which $E(Z,490) = 1\%E(0,490)$	m
Z_{90}	First optical layer $= 1/K_{d490}$	m
Θs, Theta_s	Above surface solar zenith angle	Radians

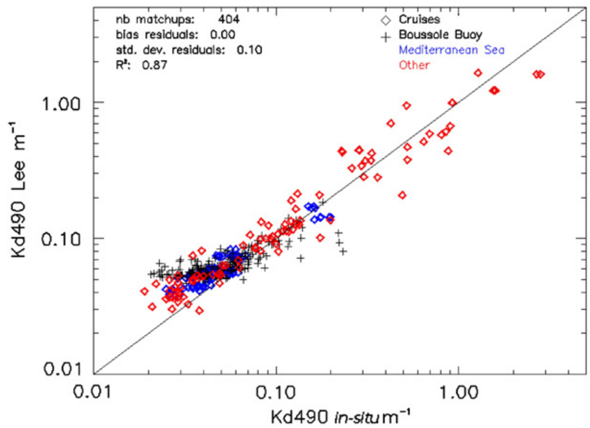

Fig. 4. Lee's K_{d490} vs. in-situ.

4. Satellite data

MERIS Level 2 Reduced Resolution (RR, 1 km resolution) data were used to match up with in-situ for the validation exercise. MERIS Full Resolution (FR) data were used to provide temporal means of Z_{eu} and K_{dPAR} over Europe. Coastal areas are characterised by strong gradients of Chl-a and SPM, which strongly affect the absorption and scattering of light. Therefore, the use of FR data when available is clearly relevant. The level 2 MERIS RR archive is available at ACRI-ST and MERIS FR data for Europe were downloaded from ESA facilities. Pixels flagged (MERIS Level 2 Detailed Processing Model) as CLOUD and HIGLINT were discarded. FR daily nLw were then projected on a regular grid of $250*250\ m^2$. Daily fields of K_{d490} and K_{dPAR} were subsequently calculated from nLw and temporally averaged over the period 2005 to 2009 as required by the EuseaMap project. Daily mean PAR (in $mol \cdot photons \cdot d^{-1} \cdot m^{-2}$) was evaluated using the algorithm developed by Frouin in 1989 and recently updated in 2011 for MERIS using Level 1 RR. The daily fields are averaged temporally over the period 2005 to 2009. Then the temporal averaged mean PAR is attenuated using the averaged K_{dPAR} at 250 m resolution and (Eq. 3) to provide an estimation of residual PAR in the water column in $mol \cdot photons \cdot m^{-2} \cdot d^{-1}$.

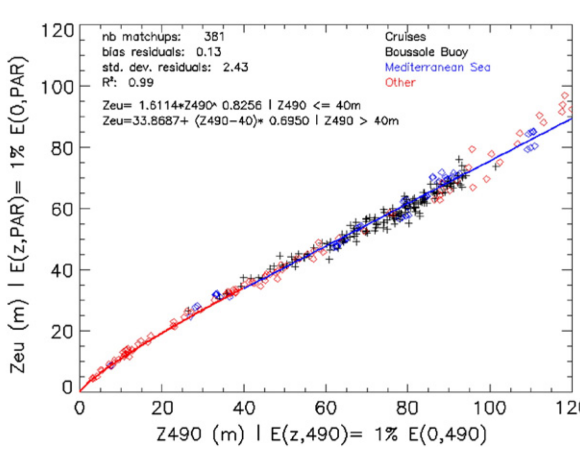

Fig. 5. Euphotic depth (Z_{eu}) related to Z_{490} (depth Z at which $E(Z,490)) = 1\%E(0,490)$ for the selected matchups.

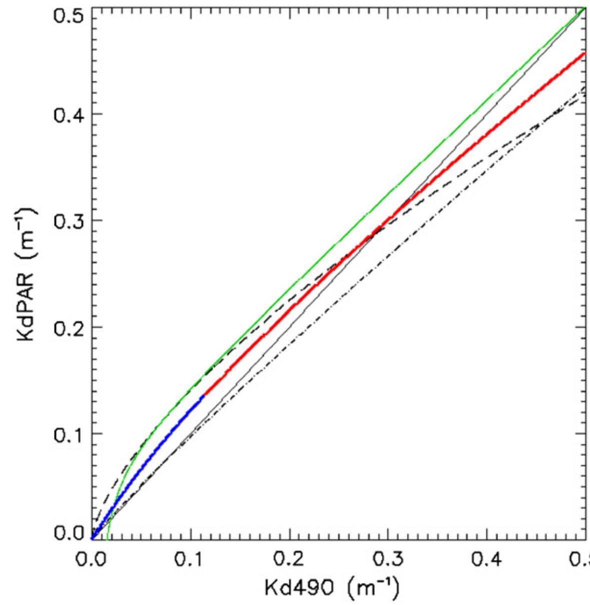

Fig. 6. Relationships between K_{dPAR} and K_{d490}. Blue curve for clear waters (Eq. 9b), red for coastal waters (Eq. 9a). The green curve shows the Morel (Eq. 10) for clear waters. The short black dotted curve for the Wang & Son's relationship for the Chesapeake bay (Eq. 11) and long black dashed line the relationship derived by Pierson and Kratzer for the Baltic Sea (Eq. 12).

5. Results

5.1. Evaluation of existing K_{d490} model compared to our in-situ dataset

5.1.1. Mueller's algorithm

Mueller (2000) proposed an empirical model for non-turbid waters based on the ratio of the nLw at wavelengths 490 and 555 nm, i.e.:

$$Kd490 = Kw490 + A(nLw490/nLw555)^B. \tag{5}$$

$K_{w490} = 0.016\ m^{-1}$ is the diffuse attenuation coefficient for pure water. Parameter A was set initially to 0.15645 and B to −1.5401. Werdell (2005a) updated (Eq. 5) to improve the algorithm performance for the clearest ocean waters. K_{w490} was suppressed, A set to 0.1853 and B set to −1.349.

Fig. 2 shows that Mueller's K_{d490} estimation is accurate for clear water ($K_{d490} < 0.2\ m^{-1}$). Above $0.2\ m^{-1}$ the algorithm saturates and the K_{d490} is clearly under-estimated compared to the dataset used. 'Other' in Fig. 2 represents matchups not collected in the Mediterranean Sea. From this same dataset, the number of matchups may vary as we progress from Figs. 2 to 7 as the spectral bands used and the algorithms may be different.

5.1.2. Morel's approach

An empirical K_{d490} model based on chlorophyll-a concentration has been proposed by Morel in 2004. This model has been recently revised (Morel et al., 2007) using in-situ measurements from the NASA Bio-Optical Marine Algorithm Dataset (NOMAD) (Werdell & Bailey, 2005a, 2005b). The revised formula is given as:

$$Kd490 = 0.0166 + 0.0773.[Chl]^{0.6715}. \tag{6}$$

Fig. 3 shows that for $K_{d490} < 0.2\ m^{-1}$, the estimated K_{d490} fits the in-situ retrievals. For turbid $K_{d490} > 0.3\ m^{-1}$ the model underestimates the attenuation. We recall that the Mueller and Morel's algorithms have been calibrated and dedicated for open sea clear waters.

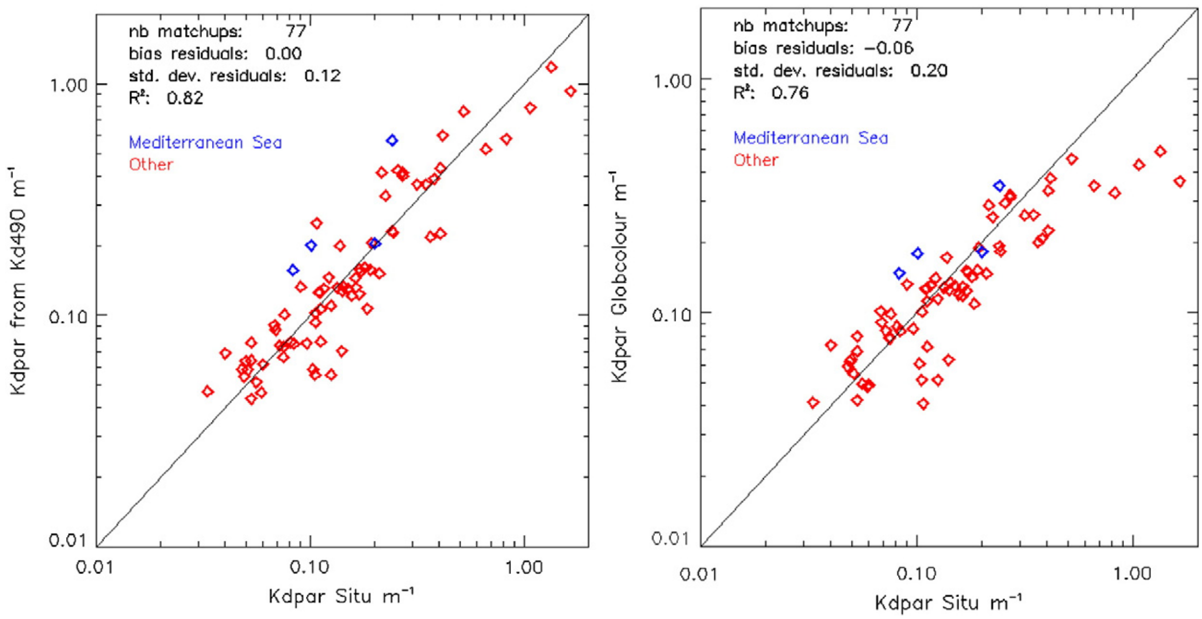

Fig. 7. a) satellite-derived K_{dPAR} from equations (Eqs. 9a and 9b) vs. in-situ K_{dPAR}. b) Globcolour standard K_{dPAR} (Eq. 10).

5.1.3. Lee's semi-analytical algorithm

Lee et al. (2005a, 2005b, 2009) proposed a semi-analytical approach to derive the mean Kd(λ) based on a radiative transfer model. The model has been revised recently (Lee et al., 2007), and Kd(λ,10%) i.e. integrated from the surface to the depth where (E(z, λ) = 10% E0(λ)) can be written as (Lee et al., 2005a):

$$Kd(\lambda, E10\%) = (1 + 0.005.\theta s).a(\lambda) + 4.18.\left(1 - 0.52.e^{-1.8\ a}\right).b_b(\lambda). \quad (7)$$

Where θs is the solar-zenith angle in the air, a(λ) the total absorption at λ and $b_b(\lambda)$ the total backscattering at λ. It is interesting to note that the semi-analytical approach developed by Lee allows the derivation of K_d at any wavelength. In our case, at λ = 490 nm, K_{d490} is derived from Eq. (7) and the absorption and backscattering coefficients at 490 nm, a(490) and $b_b(490)$ are themselves calculated using Lee's QAA v5 algorithm applied to the MERIS Rrs at wavelengths 443, 490, 555, and 670 nm.

We observe in Fig. 4 a good agreement between the satellite-derived K_{d490} and in-situ measurements between 0.06 and 1 m^{-1}. For very clear waters, K_{d490} tends to be overestimated when compared to our in-situ dataset. For in-situ K_{d490} greater than 0.08 m^{-1} the estimated K_{d490} compares well with the in-situ data.

5.2. From K_{d490} to K_{dPAR}

To derive the relationships between K_{d490} and K_{dPAR}, we have calculated using (Eq. 2b) the PAR values at the selected matchups at any depth, using a 0.1 m step for z, until PAR(z) = 1% PAR(0). $K_d(\lambda)$ at the wavelengths 412, 443, 489, 509, 559, 620, 664, and 709 were derived from Eq. (7) and applied to MERIS Rrs. $E_d(\lambda,z)$ were evaluated using Eq. (8) (Gordon & Wang, 1994), the theoretical extra-terrestrial solar irradiances $F_0(\lambda)$, the Rayleigh optical thicknesses T(λ) and the theoretical values of the ozone transmittance $T_{O3}(\lambda)$.

$$E0(z, \lambda) = F0(\lambda).\exp^{-T(\lambda)/2}.TO3(\lambda) \quad (8)$$

Two relationships were derived between Z_{eu} and the depth at which E(Z,490) = 1%E(0,490), Z_{490}, using the Lw observed at the in-situ matchups (Fig. 5). The two relationships between K_{dPAR} and K_{d490} are directly derived from the two relationships between Z_{eu} and Z_{490}. Relating K_{dPAR} to K_{d490} was not absolutely necessary as we could have integrated the spectral K_d provided by Lee using Eq. (2b). Nevertheless, we decided to propose a relationship between K_{dPAR} and K_{d490} as this link is meaningful and useful to derive K_{dPAR} from several K_{d490} in-situ datasets that are available. The threshold of 40 m for Z_{490} (K_{d490} = 0.115 m^{-1}) was set arbitrarily to separate clear from turbid waters.

An exponential model is fitted for turbid waters (Z_{490} < 40 m) and a linear model for clear waters ($Z_{490} \geq 40$ m). The proposed equations between K_{dPAR} and K_{d490} are shown in Fig. 6 (Eqs. 9a in blue and 9b in red).

$$K_{dPAR} = 4.6051.K_{d490}/(6.0700.K_{d490} + 3.200), \text{for} K_{d490} <= 0.115 m^{-1} \quad (9a)$$

$$K_{dPAR} = 0.8100.{K_{d490}}^{0.8256}, \text{for} K_{d490} > 0.115 m^{-1}. \quad (9b)$$

Morel et al. (2007) expressed K_{dPAR} as a function of Kd_{490} for clear waters:

$$K_{dPAR=}0.0665 + 0.874.K_{d490} - 0.00121/K_{d490}. \quad (10)$$

Similar approaches to Eq. (9b) have been recently developed by Wang & Son (Eq. 11, 2009) and Pierson & Kratzer (Eq. 12, 2008) for respectively the Cheasapeake Bay turbid waters and Baltic Sea, where CDOM absorption is important.

$$K_{dPAR} = 0.8045.{K_{d490}}^{0.9170} \quad (11)$$

$$K_{dPAR} = 0.6677.{K_{d490}}^{0.6763} \quad (12)$$

Relationships between K_{dPAR} and K_{d490} directly depend on [Chl-a], a_{cdom} and [SPM]. In clear waters K_{d490} values are less than K_{dPAR} values as the attenuation is greatest in the red with a resulting stronger PAR attenuation (which includes the red). In coastal areas, Pierson (2007) suggests that increasing a_{cdom} has the result of increasing more rapidly K_{d490} than K_{dPAR}.

Fig. 7 shows the scatterplot of the estimated K_{dPAR} (Fig. 7a) and the Globcolour (Fig. 7b) vs. in-situ data. The estimated K_{dPAR} is higher than the case 1 Globcolour standard algorithm for values greater than 0.3 (Fig. 6). Although the number of matchups available is small for $K_{dPAR} > 0.3\ m^{-1}$ we can observe the saturation effect on the standard K_{dPAR}. The number of available K_{dPAR} matchups is too small (Fig. 7, 77 matchups) and we propose therefore an alternative validation using Ecolight simulations (Fig. 8). The Ecolight configuration is provided in Appendix A. To obtain a realistic distribution of the IOPs we start from those gathered in the NOMAD dataset. The NOMAD dataset does not provide [SPM] and an estimation of this concentration was done using Babin et al. (2003):

$$[SPM] = 1.73/0.015.b_{bp443}. \tag{13}$$

B_{bp443} is the particular backscattering measured at 443 nm. The sun zenith angle, Θs, a required input parameter for Ecolight, was estimated for each in-situ data using the date, time, longitude and latitude. Finally the satellite-derived K_{dPAR} is compared to the K_{dPAR} estimated using Ecolight (K_{dPAR} is calculated from the PAR provided in the Ecolight output files and averaged using Eq. (4) and the depth at which $E(z) = 1\%\ E_0$).

Eqs. (9a, 9b) can also be used to derive an estimate of K_{dPAR} from K_{d490}. Fig. 9 shows a comparison for the NOMAD dataset between the K_{dPAR} estimated from the in-situ K_{d490} and the corresponding in-situ K_{dPAR}, i.e. a validation of Eqs. (9a, 9b) and Fig. 6.

Fig. 9 shows an overestimation for the very clear waters. As Lee's algorithm slightly overestimated K_{d490} for clear waters (Fig. 4) and K_{dPAR} is derived from satellite data and Lee's spectral K_d, this slight overestimation occurs for $K_{dPAR} < 0.1\ m^{-1}$, i.e. $Z_{eu} > 46$ m. For K_{dpar} greater than 0.1 m^{-1} the estimated value fits to the in-situ data (Fig. 9).

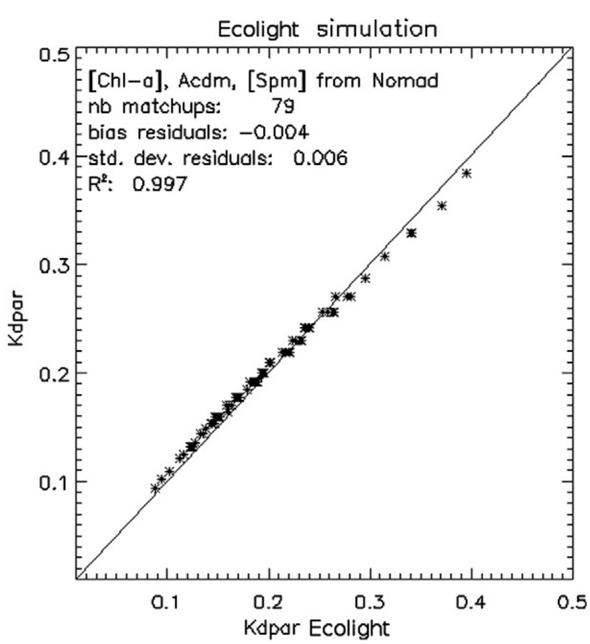

Fig. 8. Scatterplot between the Ecolight simulations and estimated K_{dPAR} based on K_{d490} by Lee et al. (2005a, 2005b).

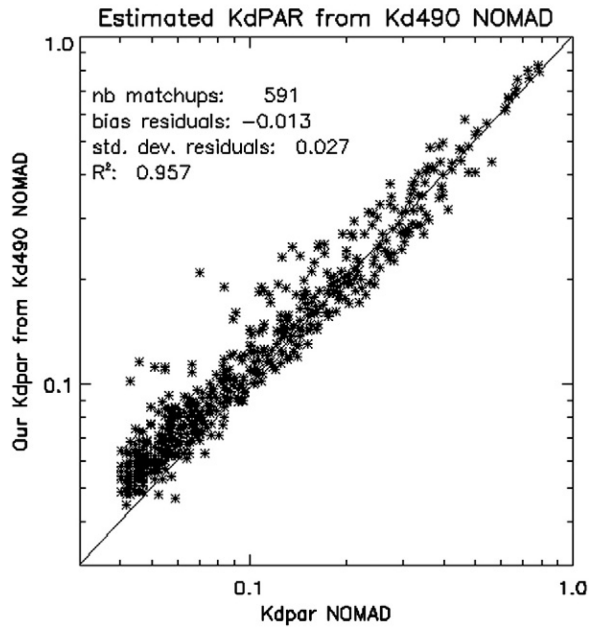

Fig. 9. Estimated K_{dPAR} from in-situ K_{d490} measurements compared to in-situ K_{dPAR}.

5.3. High resolution maps of Z_{eu} and K_{dPAR}

Fig. 10 shows the temporal mean of K_{dPAR} and Z_{eu} for Brittany and the Gulf of Lions at 250 m resolution. The covered area (Europe) by the EuSeaMap project was divided in 25 zones (not shown).

5.4. Application to seabed habitat mapping

5.4.1. P. oceanica in Corsica

In Corsica three sites where *P. oceanica* meadows are known to be in a natural state were selected for comparison. Fig. 11 shows the distribution of *P. oceanica* at two sites in north-west (Calvi) and north-east (south Bastia) Corsica. The orange line shows Z_{eu} (1% E_0) estimated from MERIS 250 m over the period 2005–2009. It is interesting to note that the lower extension for *P. oceanica* follows the satellite-derived Z_{eu}.

Gattuso et al. (2006) proposed a light range of 0.1 to 2.8 mol·photons·m^{-2}·d^{-1} for the minimum requirements of *P. oceanica*. Table 2 shows for the 3 selected sites the observed value in percentage of the surface irradiance and energy at the lower limit of the *Posidonia* beds. Using GIS software, in-situ points (black dots, Fig. 11) were selected manually on fine scale *Posidonia* maps at locations representing the deep boundary of the meadows. Statistics (Table 2) were computed for depth, percentage of the surface irradiance and energy by retrieving at these locations the values of pixels from respectively a 100 m resolution depth DTM, the temporal mean at 250 m resolution of K_{dPAR} and the temporal mean at 1 km resolution of PAR. The observed mean values, weighted means for the 3 sites by the number of observations, are 0.94% and 0.26 mol·photons·m^{-2}·day^{-1} for *P. oceanica*. These values are very close to the 1% threshold and in the lower part of the energy range proposed by Gattuso et al. (2006).

5.4.2. Kelp in Brittany

In the same manner as the previous analysis, we have evaluated the minimum light requirements for kelp using single beam sounder acoustic data acquired in 2006 and 2007 at three sites in Brittany (les Abers in North Brittany, îles de Glénan and île de Groix in South Brittany). The bathymetry used here is calculated from the

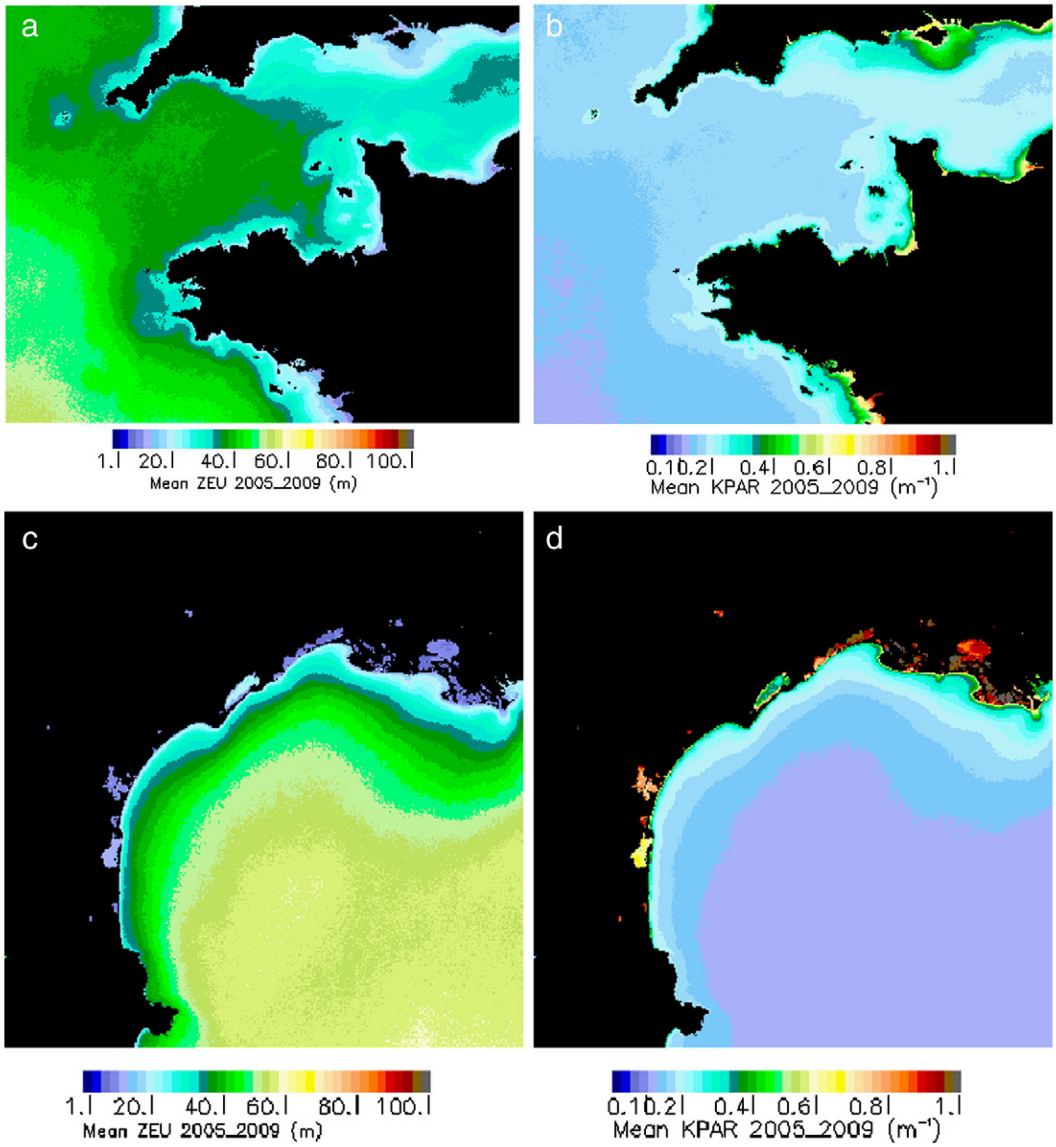

Fig. 10. Mean of Z_{eu} and K_{dPAR} at 250 m resolution over the period 2005–2009 for the Brittany (a and b) and the Gulf of Lions (c and d).

hydrographic zero, which in France corresponds to the lowest observed sea level. While in the Mediterranean Sea the tide range is very small, a tidal range of several metres in Brittany is normal. Therefore the half of the annual mean tide value at Brest (0.5∗6.1 m, Service Hydrographique et Océanographique de la Marine, SHOM) was added to the bathymetry (Table 3).

Fig. 12 shows the distribution of *L. hyperborea* in the French Abers. Kelp forest presence was obtained by echo-integrating the acoustic signal (Méléder et al., 2010), which enables distinguishing dense kelp forest from sparse kelp or bare rock. The sounder also provided in-situ depth measurements that account for the effect of tide, resulting in a relatively accurate estimate of the depth (with an uncertainty of 0.5 m). The values observed for the minimum in les Abers (mean of 2.3%) is significantly higher for the two other sites. This can be explained by the hydrodynamic energy regime at the seabed, which differs greatly between the North and South Brittany. Kain (1971, 1976) proposed a minimum percentage of incidental light ranges from 1% to 1.9% for *L. hyperborean* and Lüning (1979, 1990), 0.7% and 70 mol·m^{-2}.year^{-1} for this species, i.e. 0.19 mol·photons·m^{-2}·d^{-1}.

The calculated mean weighted values are 1.73% and 0.42 mol·photons·m^{-2}·d^{-1} in the range proposed by Kain (in fraction of surface energy) and slightly higher than the threshold approach proposed by Lüning.

6. Conclusions

We propose two relationships between the mean K_{dPAR}, integrated over the euphotic layer, and the K_{d490} estimated according to Lee et al. (2005a, 2005b), for very clear waters (K_{dPAR}<0.115 m^{-1}) and turbid waters (K_{dPAR}≥0.115 m^{-1}). The empirical relationship for coastal areas suggests a correction to the underestimation of K_{dPAR} by the standard Globcolour case 1 algorithm, and also provides an estimation of the $K_{dPAR}(Z_{eu})$ from the in-situ K_{d490}. Satellite derived K_{d490} and K_{dPAR} have been validated using available matchups between the MERIS data, in-situ measurements and Ecolight simulations. Evaluation results suggest that the Lee et al. (2005a, 2005b) algorithm derived for MERIS is valid for estimation of K_{d490} and the subsequent K_{dPAR} in coastal areas.

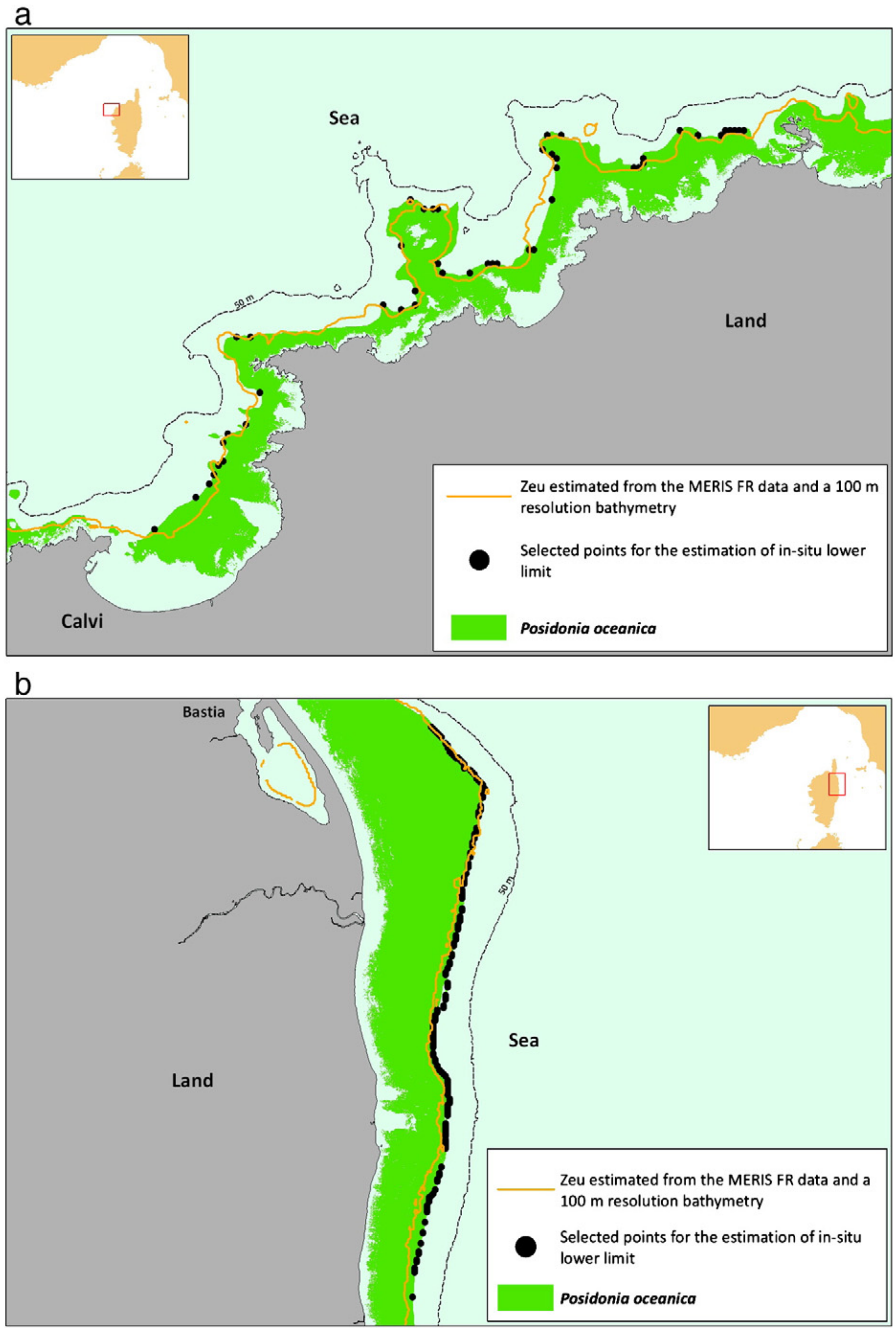

Fig. 11. Distribution of *P. oceanica* compared to Z_{eu} derived from MERIS FR daily data from 2005 to 2009 at Calvi a) and Bastia b).

The mean values of the observed threshold for the three selected sites in Corsica were 0.94% and 0.13 mol·photons·m^{-2}·d^{-1} for *P. oceanica*. These estimates are very close to the 1% definition of Z_{eu} and in the lower limit of the energy range proposed by Gattuso et al. (2006). For *L. hyperborea* surveys in Brittany, our estimated values from the satellite data were 1.73% and 0.42 mol·photons·m^{-2}·d^{-1}, in the range (1–1.9%) proposed by Kain (1971, 1976) and slightly higher than the energy threshold proposed by Lüning (0.7%, 0.19 mol·photons·m^{-2}·d^{-1} 1979, 1990). The bathymetry used in this work is calculated from the hydrographic zero, which in France corresponds to the lowest observed level of the sea. The influence of the tide has been considered in Brittany by adding the half of the mean tidal level. Bowers and Brubaker (2010) showed also that because of tide and non-linearity of the light attenuation, the light gained at low tide exceeds the loss at high tide leading to a deeper colonisation of the species in such areas. Therefore, future works will integrate accurate local estimations of annual mean tide values.

The estimation of minimum light requirements in mol·photons·m^{-2}·d^{-1}, a true physical quantity, is meaningful compared to an estimation expressed in fraction of surface energy. This residual energy reaching the bottom at high resolution is also a good candidate as input parameter in the predictive modelling of seabed habitats such as proposed by Méléder et al. (2010).

Acknowledgements

This work was funded by the EuseaMAP project http://www.jncc.gov.uk/page-5027 of the European Commission's Directorate-General

Table 2
Statistics of fraction of the surface light and corresponding energy in mol·photons·m−2·d−1 observed at the lower limit of *P. oceanica* beds.

Aléria, depth DTM accuracy: 1 m	Min	Mean	Max	St. dev.	Nb points
% E_0	0.46	**1.15**	1.92	0.20	165
mol·photons·m^{-2}·day^{-1}	0.13	**0.33**	0.56	0.06	165
Depth (m)	26.0	**31.8**	37.0	2.68	165
South Bastia, depth DTM accuracy: 1 m					
% E_0	0.4	**0.73**	1.24	0.24	171
mol·photons·m^{-2}·day^{-1}	0.12	**0.22**	0.36	0.06	171
Depth (m)	33.0	**35.4**	38.0	1.1	171
Calvi depth DTM accuracy: 5 m					
% E_0	0.44	**0.96**	2.04	0.12	48
mol·photons·m^{-2}·day^{-1}	0.13	**0.28**	0.60	0.04	48
Depth (m)	28.0	**31.0**	33.0	1.6	48

Table 3
Statistics of the fraction of surface light and the corresponding energy in mol·photons·m^{-2}·d^{-1} observed at the lower limit of *L. hyperborea* in Brittany.

Abers	Min	**Mean**	Max	St. dev.	Nb points
% E_0	1.72	**2.3**	2.74	0.43	74
mol·photons·m^{-2}·day^{-1}	0.42	**0.57**	0.68	0.11	74
Depth (m)	21.1	**22 .0**	24.7	0.65	74
Glénan					
% E_0	0.39	**0.85**	1.24	0.41	32
mol·photons·m^{-2}·day^{-1}	0.12	**0.20**	0.39	0.10	32
Depth (m)	26.0	**28.2**	32.1	1.96	32
Groix Sud					
% E_0	1.00	**1.25**	1.54	0.29	28
mol·photons·m^{-2}·day^{-1}	0.24	**0.31**	0.38	0.08	28
Depth (m)	19.1	**19.9**	21.0	0.60	28

for Maritime Affairs and Fisheries. The authors thank the SHOM and Frédéric Jourdin for providing OpticMed data and high resolution DTMs Michel Lunven from Ifremer for the provision of PAR profiles on the French shores, Robert Frouin for the provision of a revised version of the PAR estimation using MERIS data, Zhong-Ping Lee for useful advice and the Medbenth project for access to Mediterranean seagrass maps and Nick Stephens, from the Plymouth Marine Laboratory, for additional comments.

Appendix A. Hydrolight/Ecolight settings

Inherent optical properties

- Pure water absorption coefficient for 400–720 nm from (Pope and Fry, 1997)
- [Chl-a] constant with depth with values extracted from NOMAD
- Default Hydrolight Chl-a absorption coefficient
- Default Hydrolight Chl-a backscattering coefficient
- A_{cdm443} from NOMAD
- CDOM γ coefficient = −0.0176 nm^{-1}
- [SPM] from NOMAD and Eq. (13)
- Mineral particles specific scattering coefficient at 555 nm = 0.51 m^2g^{-1}
- Mineral particles specific absorption coefficient at 443 nm = 0.041 m^2g^{-1}
- Wavelengths similar to MERIS
- Chlorophyll fluorescence effects not included

Geometry

- Solar zenith angle of 40°
- Nadir viewing

Atmospheric and air–sea interface

- Surface wind speed of 5 m·s^{-1}
- Real index of refraction of water = 1.34

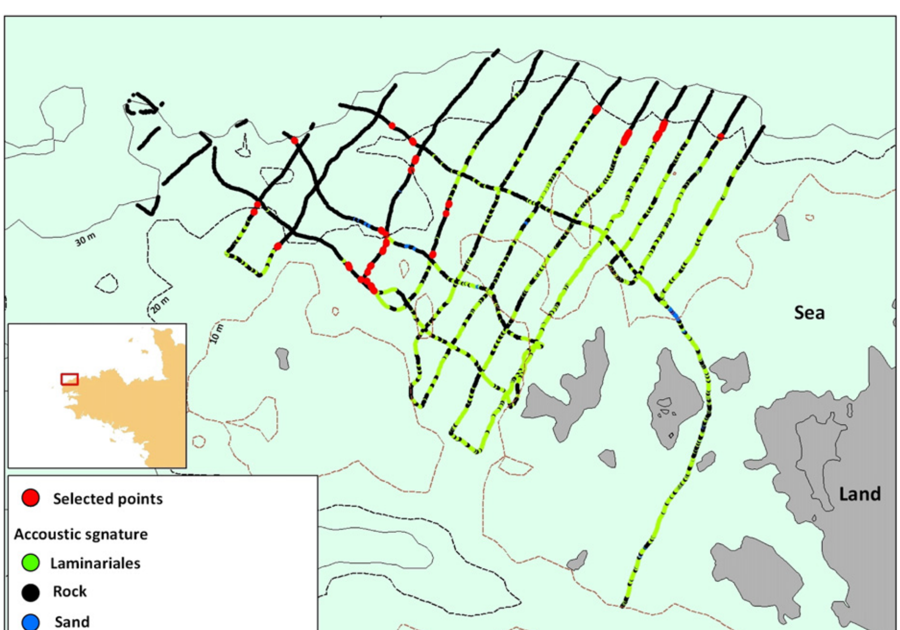

Fig. 12. Single-beam survey lines (thick lines) for the site Abers. Green dots denote the presence of kelp forest. Red dots are deepest occurrences of kelp forest.

References

Babin, M., Stramski, D., Ferrari, G. M., Claustre, H., Bricaud, A., Obolensky, G., et al. (2003). Variations in the light absorption coefficients of phytoplankton, non-algal particles, and dissolved organic matter in coastal waters around Europe. *Journal of Geophysical Research*. http://dx.doi.org/10.1029/2001JC000882.

Baker, K. S., & Frouin, R. (1987). Relation between photosynthetically available radiation and total insolation at the ocean surface under clear skies. *Limnology and Oceanography*, *32*, 1370–1377.

Barnard, A. H., Zaneveld, J. R. V., Pegau, W. S., Mueller, J. L., Maske, H., Lara, R. L., Borrego, S. A., Duarte, R. C., & Holguin, E. V. (1999). The determination of PAR levels from absorption coefficient profiles at 490 nm. *Ciencias Marinas*, *25*, 487–507.

Bowers, D. G., & Brubaker, J. M. (2010). Tidal amplification of seabed light. *Journal of Geophysical Research*, *115*, C09008.

Cahoon, L. B., Beretich, G. R., Thomas, C. J., & Mcdonald, A. M. (1993). Benthic microalgal production at Stellwagen Bank, Massachusetts Bay, USA. *Marine Ecology Progress Series*, *102*(1–2), 179–185.

Carter, C. M., Ross, A. H., Schiel, D. R., Howard-Williams, C., & Hayden, B. (2005). In situ microcosm experiments on the influence of nitrate and light on phytoplankton community composition. *Journal of Experimental Marine Biology and Ecology*, *326*, 1–13.

Claustre, H., & Maritorena, S. (2003). The many shades of ocean blue. *Science*, *302*, 1514–1515.

Devlin, M. J., Barry, J., Mills, D. K., Gowen, R. J., Foden, J., Sivyer, D., et al. (2009). Estimating the diffuse attenuation coefficient from optically active constituents in UK marine waters. *Estuarine, Coastal and Shelf Science*, *82*(1), 73–83.

Esaias, W. E., Abbott, M. R., Barton, I., Brown, O. B., Campbell, J. W., Carder, K. L., et al. (1998). An overview of MODIS capabilities for ocean science observations. *IEEE Transactions on Geoscience and Remote Sensing*, *36*(4), 1250–1265.

Falkowski, P. G., & Raven, J. A. (1997). *Aquatic photosynthesis.* Blackwell Science (349 pp.).

Frouin, R., Lingner, D. W., & Gautier, C. (1989). A simple analytical formula to compute clear sky total and photosynthetically available solar irradiance at the ocean surface. *Journal of Geophysical Research*, *94*(7), 9731–9742.

Gattuso, J. -P., Gentili, B., Duarte, C. M., Kleypas, J. A., Middelburg, J. J., & Antoine, D. (2006). Light availability in the coastal ocean: impact on the distribution of benthic photosynthetic organisms and their contribution to primary production. *Biogeosciences*, *3*, 489–513.

Gohin, F., Loyer, S., Lunven, M., Labry, C., Froidefond, J., Delmas, D., et al. (2005). Satellite-derived parameters for biological modelling in coastal waters: Illustration over the eastern continental shelf of the Bay of Biscay. *Remote Sensing of Environment*, *95*(1), 29–46.

Gordon, H. R., & Morel, A. (1983). *Remote assessment of ocean color for interpretation of satellite visible imagery: A review*, *Vol. 114*, New York: Springer-Verlag.

Gordon, H. R., & Wang, M. (1994). Retrieval of water-leaving radiance and aerosol optical thickness over the oceans with SeaWiFS: A preliminary algorithm. *Applied Optic*, *33*(3), 443–452.

IOCCG Report 3 (2000). *Remote sensing in coastal and other optically-complex waters.*

Jerlov, N. G. (1976). Optical oceanography. New York: Elsevier.

Kain, J. M. (1971). Continuous recording of underwater light in relation to Laminaria distribution. *Marine Biology Symposium* (pp. 335–346). London: Cambndge Univ. Press.

Kain, J. M. (1976). The biology of *Laminaria hyperborea*. *Oceanography and Marine Biology Annual Revue*, *17*, 101–161.

Kirk, J. T. O. (1994). *Light and photosynthesis in aquatic ecosystems.* Cambridge University Press.

Lee, Z. P. (2009). KPAR: An ambiguous optical property. *Journal of Lake Sciences*, *21*, 159–164.

Lee, Z. P., Carder, K. L., & Arnone, R. A. (2002). Deriving inherent optical properties from water color: A multiple quasi-analytical algorithm for optically deep waters. *Applied Optic*, *41*, 5755–5772.

Lee, Z. P., Darecki, M., Carder, K., Davis, C., Stramski, D., & Rhea, W. (2005). Diffuse attenuation coefficient of downwelling irradiance: An evaluation of remote sensing methods. *Journal of Geophysical Research*, *110*, C02017.

Lee, Z. P., Du, K. P., & Arnone, R. (2005). A model for the diffuse attenuation coefficient of downwelling irradiance. *Journal of Geophysical Research*, *110*, C02016.

Lee, Z. P., Lubac, B., Werdell, J., & Arnone, R. (2009). *An update of the quasi-analytical algorithm (v5)*. IOCCG software report www.ioccg.org/groups/Software_OCA

Lee, Z. P., Weideman, A., Kindle, J., Arnone, R., Carder, K., & Davis, C. (2007). Euphotic zone depth: Its derivation and implication to ocean-color remote sensing. *Journal of Geophysical Research*, *112*, C03009.

Lewis, M., Carr, M., Feldman, G., Esaias, W. E., & Mcclain, C. R. (1990). Influence of penetrating solar radiation on the heat budget of the equatorial Pacific ocean. *Nature*, *347*, 543–545.

Lüning, K. (1979). Growth strategies of three *Laminaria* species (Phaeophyceae) inhabiting different depth zones in the sublittoral region of Helgoland (North Sea). *Marine Ecology Progress Series*, *1*, 195–207.

Lüning, K. (1990). *Seaweeds: Their environment, biogeography, and ecophysiology*. New York, US: John Wiley & Sons.

McClain, C. R., Feldman, G. C., & Hooker, S. B. (2004). An overview of the SeaWiFS project and strategies for producing a climate research quality global ocean bio-optical time series. *Deep Sea Research Part II*, *51*, 5–42.

Mcminn, A., Hirawake, T., Hamaoka, T., Hattori, H., & Fukuchi, M. (2005). Contribution of benthic microalgae to ice covered coastal ecosystems in northern Hokkaido, Japan. *Journal of the Marine Biological Association of the United Kingdom*, *85*(2), 283–289.

Méléder, V., Populus, J., Guillaumont, B., Perrot, T., & Mouquet, P. (2010). Predictive modelling of seabed habitats: Case study of subtidal kelp forests on the coast of Brittany, France. *Marine Biology*, *157*(7), 1525–1541.

MERIS level 2 detailed processing model. http://earth.esa.int/pub/ESA_DOC/ENVISAT/MERIS/MERIS_DPML2_i7r2A_re-issued.pdf

Morel, A. (1988). Optical modeling of the upper ocean in relation to its biogenous matter content. *Journal of Geophysical Research*, *93*, 10749–10768.

Morel, A., Antoine, D., & Gentili, B. (2002). Bidirectional reflectance of oceanic waters: Accounting for Raman emission and varying particle phase function. *Applied Optics*, *41*, 6289–6306.

Morel, A., Huot, Y., Gentili, B., Werdell, P. J., Hooker, S. B., & Franz, B. A. (2007). Examining the consistency of products derived from various ocean color sensors in open ocean (Case 1) waters in the perspective of a multi-sensor approach. *Remote Sensing of Environment*, *111*, 69–88.

Morel, A., & Smith, R. C. (1974). Relation between total quanta and total energy for aquatic photosynthesis. *American Society of Limnology and Oceanography*, *19*(4), 591–600.

Mueller, J. L. (2000). SeaWiFS algorithm for the diffuse attenuation coefficient, K_{d490}, using water-leaving radiances at 490 and 555 nm. *SeaWiFS Postlaunch Technical Report Series*Greenbelt, Maryland: NASA Goddard Space Flight Center (24–27 pp.).

Pierson, D. C., Kratzer, S., Strombeck, N., & Hakansson, B. (2008). Relationship between the attenuation of downwelling irradiance at 490 nm with the attenuation of PAR (400 nm– 700 nm) in the Baltic Sea. *Remote Sensing of Environment*, *112*, 668–680.

Pope, R. M., & Fry, E. S. (1997). Absorption spectrum (380–700 nm) of pure water. II. Integrating cavity measurements. *Applied Optics*, *36*, 8710–8723.

Rochford, P. A., Kara, A. B., Wallcraft, A. J., & Arnone, R. A. (2001). Importance of solar subsurface heating in ocean general circulation models. *Journal of Geophysical Research*, *106*, 30923–30938.

Ryther, J. H. (1956). Photosynthesis in the ocean as a function of light intensity. *Limnology and Oceanography*, *1*, 61–70.

Sathyendranath, S., Gouveia, A. D., Shetye, S. R., Ravindran, P., & Platt, T. (1991). Biological control of surface temperature in the Arabian Sea. *Nature*, *349*, 54–56.

Wang, M., & Shi, W. (2005). Estimation of ocean contribution at the MODIS near-infrared wavelengths along the east coast of the U.S.: Two case studies. *Geophysical Research Letters*, *32*, L13606.

Wang, M., Son, S., & Harding, L. (2009). Retrieval of diffuse attenuation coefficient in the Chesapeake Bay and turbid ocean regions for satellite ocean color applications. *Journal of Geophysical Research*, *114*, c10011.

Werdell, P. J., & Bailey, S. W. (2005a). An improved bio-optical data set for ocean color algorithm development and satellite data product validation. *Remote Sensing of Environment*, *98*(1), 122–140.

Werdell, P. J., & Bailey, S. W. (2005b). *NASA technical memorandum 104566*, *vol. 25*.

Wu, Y., Tang, C., Sathyendranath, S., & Platt, T. (2007). The impact of bio-optical heating on the properties of the upper ocean: A sensitivity study using a 3-D circulation model for the Labrador Sea. *Deep Sea Research Part II*, *54*, 2630–2642.

Zaneveld, J. R. V., Kitchen, J. C., & Mueller, J. L. (1993). Vertical structure of productivity and its vertical integration as derived from remotely sensed observations. *Limnology and Oceanography*, *38*, 1384–1393.